LA-UR-97-1234

Title:

Response of a Water-Filled Spherical Vessel to an Internal Explosion

Author(s):

Tim Wilson
Matthew Lewis

Submitted to:

Response of a Water-Filled Spherical Vessel to an Internal Explosion

Tim Wilson and Matthew Lewis
Los Alamos National Laboratory
twilson@lanl.gov, mlewis@lanl.gov

I. INTRODUCTION

Many problems of interest to the defense community involve fluid-structure interaction (FSI). Such problems include underwater blast loading of structures, bubble dynamics and jetting around structures, and hydrodynamic ram events. These problems may involve gas, fluid, and solid dynamics, nonlinear material behavior, cavitation, reaction kinetics, material failure, and nonlinearity that is due to varying geometry and contact conditions within a structure or between structures.

To model such problems in two-dimensions we developed the FSI2D code by coupling MFICE2D [1, 2], a Los Alamos finite volume computation fluid dynamics (CFD) code, with PRONTO2D [3], a SANDIA finite element solid dynamics code. Details on this coupling approach and current implementations are discussed in Section III.

In this report we use FSI2D to model the response of "Jumbino," a water-filled spherical steel vessel (63.4 cm i.d., 6.1 cm wall thickness), to an internal explosion caused by detonating 30 grams of C-4 at the center of the vessel.

Predictions from a fully coupled model were compared to experimental results in the form of strain gauge traces. Agreement was reasonably good. Additionally, the calculation was run in an uncoupled mode to understand the importance of fluid-structure interaction in this problem. The uncoupled model results in an accumulation of nonphysical energy in the vessel.

II. PROBLEM DESCRIPTION

A drawing of the Jumbino vessel shown in Fig. 2.1. One end of the vessel (the right end in the figure) was sealed with a one inch thick Plexiglas plug. A steel plug was bolted in the other end as shown in the figure. The vessel is made of A537 structural steel, with an estimated yield strength of 40,000 psi.

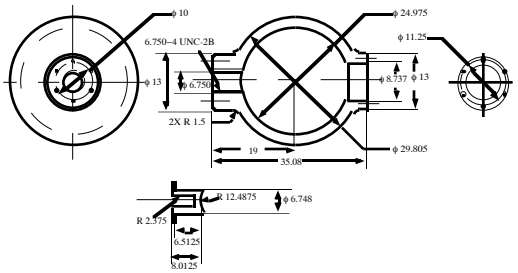

Fig. 2.1 Engineering sketch of the Jumbino vessel. The steel plug inserted into the left (as shown) end is shown below the sketch. All dimensions are in inches.

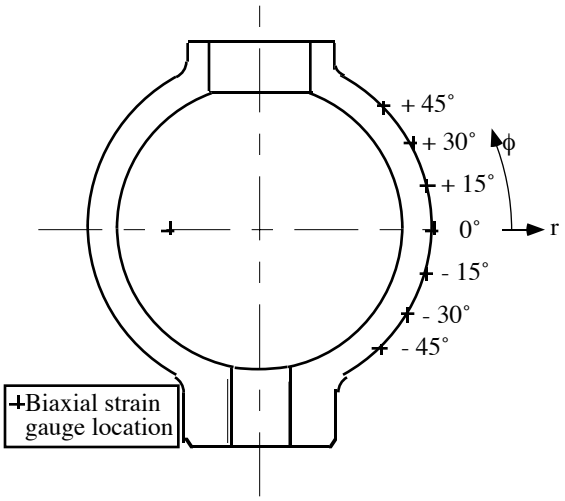

Figure 2.2 An engineering sketch of the Jumbino vessel indicating strain gauge locations. Two strain gauges were at each location shown, one latitudinal (or hoop) gauge and one longitudinal gauge.

One-quarter inch strain gauges were placed on the outside of the vessel to record the azimuthal and meridional components of the vessel motion. These strains, referred to here as the hoop and longitudinal components, respectively, are principal strains in an ideally axisymmetric problem. Gauges were affixed at seven locations along the $\theta = 0$ meridian at 15° ϕ intervals from -45° to +45° and at three

locations around the equator (z = 0) at 120° θ intervals as indicated in Fig. 2.2.

III. NUMERICAL FSI METHODOLOGY

A fully implicit numerical coupling of the fluid and solid solutions facilitates a physically coupled solution. The CFD algorithm is discussed in Kashiwa et al. [1, 2] and by Lewis et al. [4] and details of the solid dynamics algorithm are discussed in Taylor and Flanagan [3].

Nodes on the surface of the structural domain are required to be coincident with vertices on the surface of the fluid domain. Pressure and velocity data are exchanged on the faces defined by these points and at these points.

A new feature of FSI2D, demonstrated in the present analysis, is the capability of running a problem in either a fully coupled mode (coupled for short) or in an uncoupled mode. In the coupled mode, where the particle normal velocity is continuous across the interface, an iterative approach is used to force the pressure field and the structural accelerations to be compatible. In this mode, the physical fluid-structure interface moves; that is, the fluid domain changes as the structure deforms, translates, and rotates. Momentum and energy are conserved. In the uncoupled mode, the fluid-structure interface is treated as a rigid boundary when the fluid equations are solved. Pressures so calculated are then used as boundary conditions to the structure, which then deforms. Momentum and energy are *not* conserved.

IV. COMPUTATIONAL MODEL

A. Fluid Domain. An axisymmetric cylindrical coordinate system is used to describe the geometry of the Jumbino experiment where (r, θ, and z) are the radial, azimuthal, and axial coordinates that form a right-handed coordinate system. The angle ϕ, measured counterclockwise from the r-axis in the meridional plane, denotes the angle of latitude.

The interior of the vessel, known hereafter as the fluid domain, is discretized with 4279 quadrilateral cells in eight logically rectangular blocks as shown in Fig. 4.1.
At the instant of detonation, the water is motionless and in hydrostatic equilibrium with the ambient atmosphere. A Us-Up equation of state is used to model the water [5, p. 391] and a Becker-Kistiakowsky-Wilson (BKW)-gas equation of state is used to model the explosive [5].

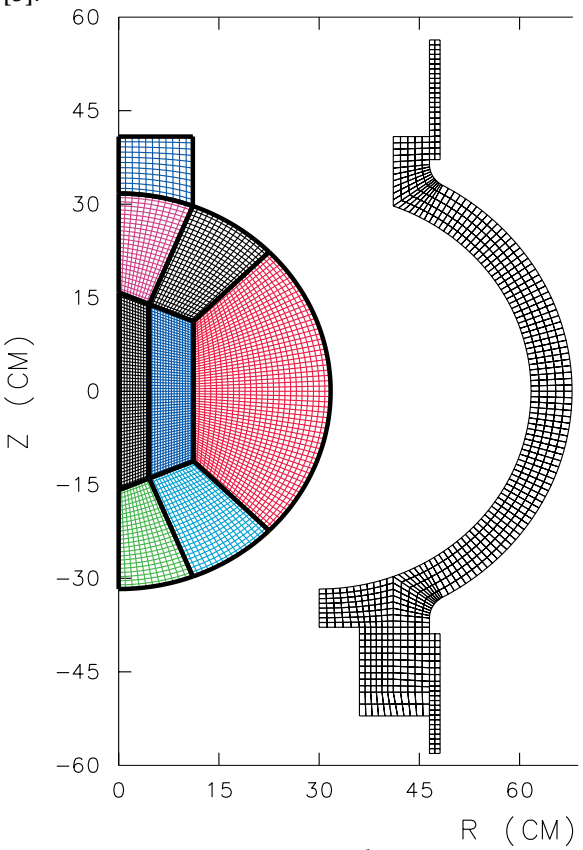

Fig. 4.1 Computational mesh for fluid and solid domains.

Boundary conditions are straightforward. Along the z-axis the axisymmetric condition is modeled as a reflective surface, the water-Plexiglas interface at the top of the port is modeled as an outflow (zero normal gradient) surface and the water-vessel interface is modeled with the FSI model described in Section III.

B. Jumbino Vessel. The steel vessel, shown radially offset from the fluid in Fig. 4.1, is discretized with 765 quadrilateral finite elements. Compliance of the support structure is modeled by including elements that provide

an additional mass of 1.997 kg and an axial stiffness of 30.873 x 10^4 N/cm.

V. TWO-DIMENSIONAL FSI CALCULATIONS AND EXPERIMENTAL RESULTS

In this section we describe the results of the Jumbino experiment and compare them with a pair of two-dimensional numerical simulations. In Sections V.A and V.B is a description of the time and space dynamics of the coupled calculation. Comparison and analysis follow in Sections V.C and V.D. Unless noted otherwise, reported quantities are for the coupled calculation.

A. Fluid Time Evolution. The dynamics of the problem are driven by the high explosive. During the time period of interest the bubble expands, contracts, and then expands again as a function of its own energy and the momentum of the surrounding water (Fig. 5.1). In turn, the motion of the water is then affected by resistance and motion of the Jumbino vessel. During the initial bubble expansion the water motion is outward nearly everywhere; during the subsequent bubble contraction the water motion is inward nearly everywhere.

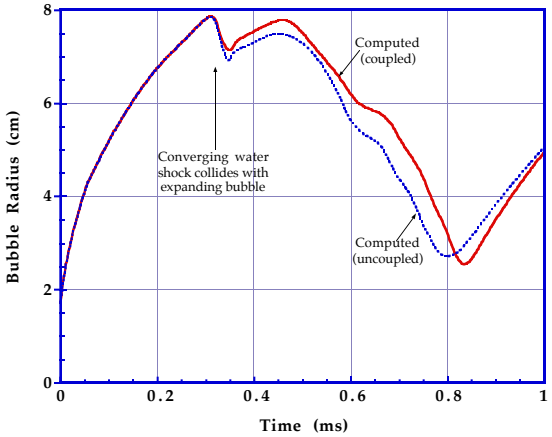

Fig. 5.1 HE-gas bubble radius.

In the first 0.310 ms, the high temperature and pressure HE cylinder rapidly expands 112-fold at an average rate of 20 cm/ms to its maximum size, a nearly spherical gas bubble with a radius of 7.9 cm (V = 2042 cm^3). During this time the temperature and pressure drop from 2714 K and 152.7 kbars to 300 K and 15 bars, driving a quasi-spherical shock into the surrounding water. The water shock reflects off the vessel wall, generating peak pressures of about 680 bars (t = 0.190 ms). The expanding bubble generates a second pressure wave that reaches the wall at t = 0.420 ms, producing peak pressures of about 450 bars. The bubble expands until t = 0.310 ms, contracts briefly when hit with the now converging first shock, re-expands until t = 0.458 ms, and then collapses because the water is moving inward nearly everywhere.

Away from the port (the Plexiglas covered opening at the top of vessel) the flow remains approximately spherical until the problem end time (t = 1.0 ms). Figure 5.2 shows the pressure at the vessel wall at the time of the first and second maxima on the equator. Away from the port, p vs. ϕ for the first shock is spherically symmetric; that is, the top curve in Fig. 5.2 should be horizontal. For the fluid mesh used here (Fig. 4.1), an expanding spherical wave first traverses a ϕ-dependent thickness of square mesh cells before reaching the outer cylindrical mesh. The dip in p ($-35° < \phi < +35°$) is thus an artifact of mesh geometry. Although a smoother mesh would produce a more nearly one-dimensional solution, the asymmetry of the present calculation (6% at the equator) is not large enough to alter the principal dynamics of interest here.

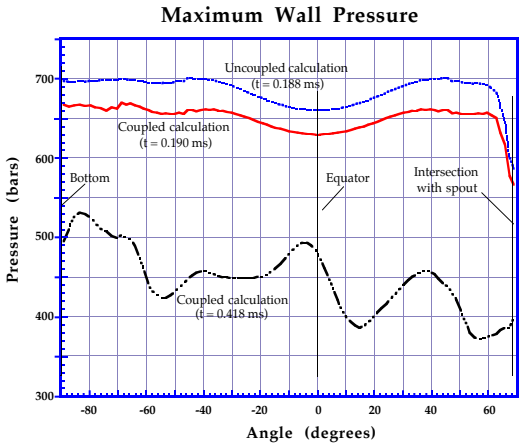

Fig. 5.2 Fluid pressure at the vessel wall (at the time of maxima on the equator).

At midradius the water accelerates to a maximum velocity of 6.1 cm/ms (t = 0.100 ms, r = 15 cm), and the shock front reaches the top of the circular port at t = 0.200 ms. Water is

pushed through the port opening during the next 0.8 ms at an average rate of 1.9 cm/ms, giving a net mass egress of 588 g at t = 1.0 ms.

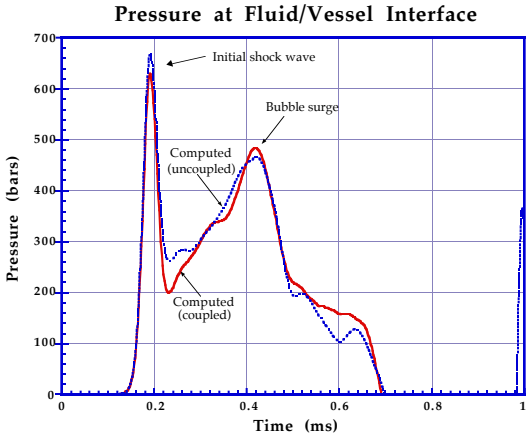

Fig. 5.3 Fluid pressure at the vessel wall (z = 0).

Figure 5.3, which shows the pressure time-history of the fluid adjacent to the vessel wall at $\phi = 0$, is typical of other wall locations.

B. Vessel Time Evolution. The primary dynamical response of the vessel is radial—a sequence of expansions and contractions initiated by the nearly spherical internal shock and maintained by a balance of fluid pressure and elastic forces. Three maxima are observed in the outward motion of the vessel with outward radial displacements at the equator of 0.0165 cm (t = 0.275 ms), 0.0133 cm (t = 0.518 ms), and 0.0053 cm (t = 0.774 ms). The motion of the fluid and the vessel are clearly coupled until t = 0.7 ms as evidenced by sustained wall pressures above 100 bars. For t > 0.7 ms sufficient relief, caused mostly by the bubble contraction and to a lesser degree by water egress, allows the remaining water to move around without forced contact with the vessel.

C. Comparison of Measured and Computed Vessel Strains. Typical strain time-histories, at ($\phi = -45°$, $\theta = 0°$), are shown in Figures 5.4 and 5.5. Both plots show three curves representing the measured, coupled and uncoupled computed values. The time scale is keyed to the calculated values where the HE detonation occurs at t = 0. The measured values lag the computed values by 0.060 ms at the $+\phi$ locations and by about 0.020 ms at $-\phi$ locations. For purposes of comparison, all measured values were shifted by -0.060 ms.

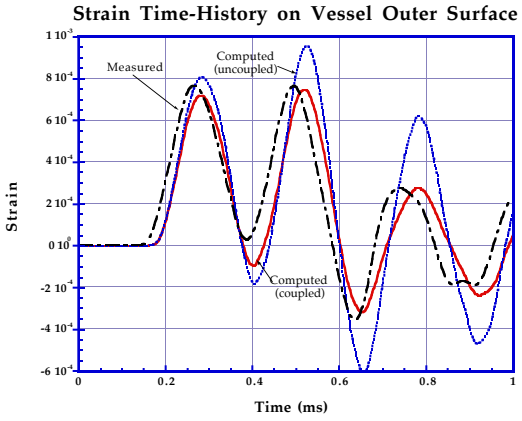

Fig. 5.4 Hoop strain at $\phi = -45°$ and $\theta = 0°$.

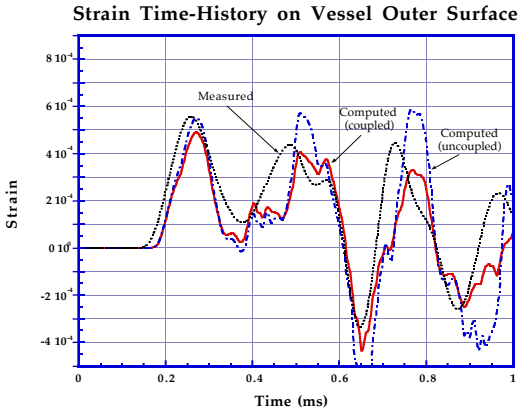

Fig. 5.5 Longitudinal strain at $\phi = -45°$ and $\theta = 0°$.

Generally, the calculated strains compare well with the measured values. Analysis of the hoop strain data reveals the observations that follow.

1. The computed peak-to-peak timing is very nearly the same as the measured values on all plots, a fact which indicates that the FSI model adequately models the timing of the hydrodynamics and the hoop forces in the vessel.

2. All three traces show the initial expansion caused by the first shock, contraction to near the original radius, re-expansion caused by the bubble surge, and a third peak. The time between the second and third peaks, 0.287 ms, compares well with the estimated natural period of the vessel, 0.253 ms.

3. All three traces show that peak strains are smallest on the equator and get progressively larger away from the axis. The traces also correlate between plus and minus ϕ locations.

4. During the first oscillation, the uncoupled strains compare better with the measured values than do the coupled strains; however, the reverse is true at later times. An explanation for this turnaround is offered in Section V.D. For the time up to the first peak and for a short time thereafter, the dynamics are almost purely one-dimensional and unaffected by the complex interaction and reflection of shocks that occur later and by the vessel vibration modes excited by asymmetric structural boundary conditions.

5. After the first peak, uncoupled strains are damped *less* than the coupled and measured values; this is especially notable for $t > 0.6$ ms. The reason for this difference in damping becomes clearer if we consider the time-dependent energy balance in the elastic vessel (Section V.D).

Generally speaking, these trends are also evident in the longitudinal strain data (Fig. 5.5). The longitudinal waveforms have more structure because (a) there is additional mass at the poles and (b) the vessel is clamped to the support frame at the poles. The major dynamical effect is to lower longitudinal strains (compare with hoop strains) and to introduce higher frequencies into the longitudinal motion. The latter is especially apparent for the computed values.

D. Vessel Energy. For the coupled calculation, Fig. 5.6 shows the internal and kinetic energies of the vessel as a function of time. The vessel energies are due to the mechanical work done by the fluid on the vessel wall (lower curve). During the loading period ($t < 0.7$ ms) the vessel oscillates twice as is readily apparent in the two prominent cycles in the internal energy and pdV work curves. After $t = 0.7$ ms, fluid pressure at the surface is essentially zero and no further energy is exchanged between the fluid and vessel; hence, the pdV curve is constant.

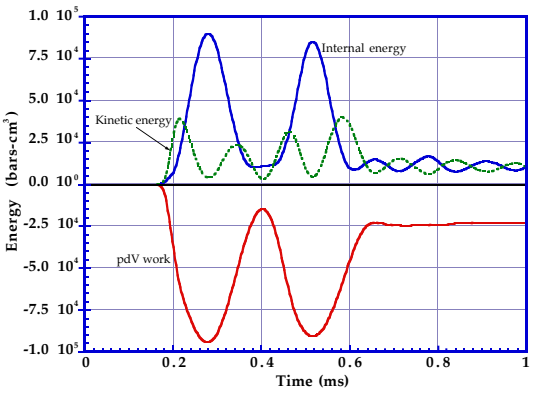

Fig. 5.6 Structural energy balance for coupled calculation.

The total vessel energies (internal + kinetic) are plotted in Fig. 5.7 for both cases. The difference between the uncoupled and coupled calculations (dE_t) is shown in the bottom curve. For $t < t_m$, p(t) is the initial shock wave and dE_t increases steadily. For later times, p(t) is a complicated function of wave interactions and FSI; moreover, it is not at all apparent from looking at the two p(t) curves (Fig. 5.3) what form of dE_t to expect. During the first vessel contraction, dE_t actually decreases, nearly compensating for all the previously accumulated error. However, during the second oscillation, dE_t increases on both expansion and contraction so that by the time p(t) = 0, the steady-state vessel energy for the uncoupled case is nearly 3 times the coupled energy. Thus, we expect steady-state stresses to differ by approximately a factor of $\sqrt{3}$.

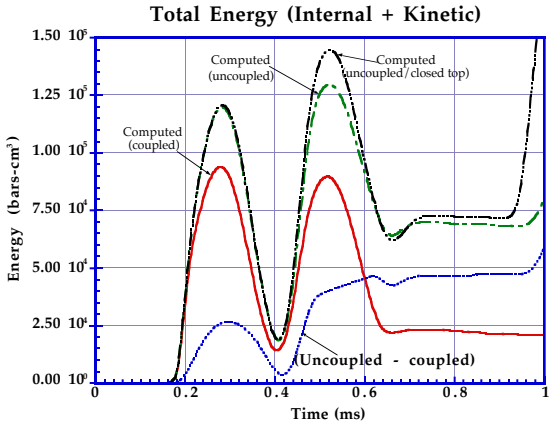

Fig. 5.7 Total structural energy for coupled and two uncoupled calculations.

For the Jumbino experiment, the large differences in late-time vessel energy are the most dramatic illustration of the importance of modeling fluid-structure interaction in a fully coupled manner, compared with a more traditional uncoupled treatment. Even though the uncoupled strains are closer to the measured values (which are assumed to be accurate) than are the coupled strains during the first oscillation, the accumulation of nonphysical energy causes the uncoupled values to diverge significantly from the measured values at later times. An uncoupled method is always nonconservative, and the vessel will acquire nonphysical energy for any p(t) scenario of the general type considered here.

VI. CONCLUSIONS

In this report we have examined the dynamical response of a water-filled spherical steel vessel, having a nominal radius of 34.8 cm, a wall thickness of 6.1 cm, and a fundamental period of 0.253 ms, subjected to a centrally detonated 30 g charge of C-4 high explosive. The resultant pressure loading in the range of a few hundred bars lasted 0.550 ms and pushed the vessel radially outward about 0.02 cm, generating peak strains of about 6×10^{-4}. Vessel hoop strain time-histories computed by the FSI2D hydrodynamics code compared well with experimental data.

Our computational analysis focused on the fluid-structure interaction aspects of the problem, specifically, on two models. The first model treats the motion of the fluid and solid together in a physically based manner giving a fully *coupled* solution. The second model—the *uncoupled* case—computes the fluid field with a rigid wall boundary condition. The resulting fluid pressure at the wall is then applied to the vessel as a boundary condition. The coupled model conserves momentum and energy, continuously exchanging both quantities between the fluid and solid during vessel expansion and contraction. The uncoupled model, by contrast, does none of these things.

The uncoupled loading resulted in a nonphysical accumulation of energy in the vessel as evidenced by strain traces that were less damped than and diverged from experimental traces. After the pressure loading, the steady-state vessel energy in the uncoupled model was three times greater than the coupled vessel energy.

Further, results were consistent with a pair of simple one-dimensional models [6].

REFERENCES

1. B. A. Kashiwa, N. T. Padial, R. M. Rauenzahn, W. B. VanderHeyden, "A Cell-Centered ICE Method for Multiphase Flow Simulations," Los Alamos National Laboratory document LA-UR-93-3922 (rev.), presented at the ASME Symposium on Numerical Methods for Multiphase Flows, Lake Tahoe, Nevada, June 19-23, 1994 .

2. B. A. Kashiwa, R. M. Rauenzahn, "A Multimaterial Formalism," Los Alamos National Laboratory document LA-UR-94-771, presented at the ASME Symposium on Numerical Methods for Multiphase Flows, Lake Tahoe, Nevada, June 19-23, 1994.

3 L. M. Taylor and D. P. Flanagan, "PRONTO2D: A Two-Dimensional Transient Solid Dynamics Program," Sandia National Laboratories report SAND86-0594 (March 1987).

4 M. W. Lewis, B. A. Kashiwa, R. W. Meier, and S. Bishop, "Nonlinear Dynamic Fluid-Structure Interaction Calculations with Coupled Finite Element and Finite Volume Programs," presented at the ASME Winter Annual Meeting, Chicago, Illinois, November 6-11, 1994, Los Alamos National Laboratory document LA-UR-94-2443.

5. C. L. Mader, *Numerical Modeling of Detonations* (University of California Press, Berkeley, 1979).

6. M.W. Lewis and T.L. Wilson, "Response of a Water-Filled Spherical Vessel to an Internal Explosion," Los Alamos National Laboratory report LA-13240-MS (1997).